



# Transition prediction for re-entry capsules with intermittency-based RANS models

Luigi Cutrone, Francesco Cascone, Antonio Schettino<sup>3</sup>

#### **Abstract**

The prediction of boundary-layer transition in hypersonic flows is a critical challenge in aerodynamic design, influencing heating rates, skin friction, and overall vehicle performance. The transition process, governed by a complex interplay of instability mechanisms, is particularly relevant for atmospheric entry capsules and hypersonic vehicles, where accurate modeling is essential for thermal protection system (TPS) design. Moreover, in high-enthalpy conditions, the boundary-layer stability is strongly influenced by chemical and thermal non-equilibrium phenomena, including wall catalysis. To address these complexities, this study evaluates intermittency-based transition models within the Reynolds-Averaged Navier-Stokes (RANS) computational fluid dynamics (CFD) framework, incorporating non-equilibrium effects to improve transition prediction.

**Keywords:** hypersonic transition, intermittency model, RANS, turbulence

#### **Nomenclature**

Latin St – Stanton number Tu - Turbulence intensity Turbulent kinetic energy  $P_k$  - Production term in k equation Greek  $E_k$  – Destruction term in k equation - Intermittency factor  $\begin{array}{ll} P_{\gamma} & - \text{ Production term for intermittency} \\ E_{\gamma} & - \text{ Destruction term for intermittency} \\ Re & - \text{ Reynolds number} \end{array}$  $\mu_t$  – Eddy viscosity  $\lambda_{\theta_L}$  – Local pressure gradient parameter  $\mathrm{Re}_V$  – Vorticity-based Reynolds number,  $\frac{\rho d_w^2 S}{\mu}$ Subscripts  $\tilde{R}e_{\theta}$  – Momentum-thickness Reynolds number, eL – At boundary layer edge  $\rho\theta U$ w – Wall  $Re_{\theta_c}$  – Critical Reynolds number based on momen- $\infty$  – Free-stream tum thickness *fr* – Fay-Riddel

# 1. Introduction

The prediction of boundary-layer transition in hypersonic flows remains one of the most critical and challenging tasks in aerospace engineering. Transition strongly affects convective heat transfer, skin friction, and ultimately the aerothermodynamic loads experienced by a vehicle. An accurate assessment of transition onset and progression is therefore a key enabler for the design of thermal protection systems (TPS) and the optimization of vehicle performance during atmospheric entry.

For re-entry capsules and hypersonic vehicles, the problem is further complicated by the wide range of instability mechanisms that can trigger transition. Depending on local flow conditions, disturbances may grow due to first-mode or second-mode instabilities, crossflow effects, or other mechanisms such

<sup>&</sup>lt;sup>1</sup>Italian Aerospace Research Center, l.cutrone@cira.it

<sup>&</sup>lt;sup>2</sup>Italian Aerospace Research Center, f.cascone@cira.it

<sup>&</sup>lt;sup>3</sup>Italian Aerospace Research Center, a.schettino@cira.it

as nose bluntness and surface roughness. In high-enthalpy environments, chemical and thermal non-equilibrium, as well as wall catalysis, can significantly alter stability properties, making transition prediction even more complex.

Traditional approaches based on linear stability theory (LST) or parabolized stability equations (PSE) have proven effective for canonical configurations, while their application to three-dimensional, complex geometries encountered in real vehicles is often impractical. In this context, transition models embedded within Reynolds-Averaged Navier–Stokes (RANS) frameworks offer a more tractable alternative for engineering design, allowing the simulation of full configurations while capturing transition effects in an approximate but computationally efficient manner.

A promising class of such approaches is represented by intermittency-based models, in which the intermittency factor  $\gamma$  is introduced to describe the temporal and spatial fraction of turbulence in transitional boundary layers. Early formulations by Suzen et al. [14] and Steelant and Dick [13] provided the foundation for these methods, although they relied on non-local correlations. More recently, Langtry and Menter [3] proposed the Local Correlation-based Transition Modeling (LCTM) framework, which has inspired a new generation of local, correlation-driven models. Among these, the Smirnov–Menter model [10] and the Liu et al. model [5] are particularly relevant, as they extend applicability to hypersonic regimes and account for different transition mechanisms, including streamwise and crossflow instabilities.

Despite these advances, the robustness and accuracy of intermittency-based RANS models across a variety of hypersonic conditions and geometries remain active research questions. To address this, the present work evaluates selected transition models in configurations of increasing complexity, from flat plates at different Reynolds numbers to the BOLT demonstrator and the Hypersonic Inflatable Aerodynamic Decelerator (HIAD) aeroshell. The objective is to assess the predictive capability of these models in both canonical and applied test cases, with emphasis on their sensitivity to free-stream conditions, turbulence intensity, and numerical settings.

# 2. Governing Equations

RANS-coupled transition models are often associated with an intermittency transport equation, such as the one initially formulated by Suzen et al. [14], or a more complex formulation as that proposed by Steelant and Dick [13]. The intermittency factor  $\gamma$  represents the relative fraction of time that turbulent spots are present at a given spatial location within the transitional flow. It is therefore a measure of the progress of the transition process from a laminar to a turbulent flow in the boundary layer. The above-mentioned models [14, 13], however, rely on non-local information to induce the onset of transition. In 2009, Langtry and Menter [3] introduced a Local Correlation-based Transition Modeling (LCTM) framework to address this issue. Building upon this initial model, several new models were subsequently developed. In this class of models, the transport equation for the intermittency  $\gamma$  is generally formulated as follows:

$$\frac{\partial \rho \gamma}{\partial t} + \frac{\partial \left(\rho u_j \gamma\right)}{\partial x_j} = P_{\gamma} - E_{\gamma} + \frac{\partial}{\partial x_j} \left[ \left(\mu + \mu_t\right) \frac{\partial \gamma}{\partial x_j} \right]. \tag{1}$$

where  $P_{\gamma}$  and  $E_{\gamma}$  are the production and the destruction terms for  $\gamma$ :

$$P_{\gamma} = c_{a_1} F_{\text{length}} \rho S \left( \gamma F_{\text{onset}} \right)^{c_b} \left( 1 - c_{e_1} \gamma \right), \quad E_{\gamma} = c_{a_2} \rho \Omega \gamma F_{\text{turb}} \left( c_{e_2} \gamma - 1 \right). \tag{2}$$

The solution of the above equations relies on a series of calibration coefficients, the values of which depend on the model selection. These values will not be provided in this study; readers are encouraged to refer to the relevant publication for further details.

The intermittency factor  $\gamma$  obtained from Eq. (1) is used to control the production and destruction terms in the turbulent kinetic energy equation of a  $k-\omega$  SST turbulence model:

$$\tilde{P}_k = \gamma P_k, \quad \tilde{E}_k = \max\left[\gamma, 0.1\right] E_k.$$
 (3)

In addition, the blending function  $F_1$  in the  $k-\omega$  SST turbulence model, [8], is modified for transition simulations according to Langtry and Menter [3].

# 2.1. Smirnov, Menter 2015

The intermittency transition model proposed by Smirnov and Menter in 2015 [10] is a further development based on the 2009 Langtry and Menter  $\gamma-\tilde{\mathrm{Re}}_{\theta_t}$  transition model which solves only one transport equation for the turbulence intermittency and avoids the need for the second differential equation. The model was initially developed to take only streamwise (i.e. in the direction of the main flow) transition into account but it was later expanded to incorporate crossflow transition as well [9]. The function  $F_{\mathrm{onset}}$  is here evaluated by taking the maximum value between the streamwise and crossflow contributions, computed as follows:

$$F_{\mathsf{onset},\mathsf{s}} = \frac{\mathsf{Re}_V}{2.2\mathsf{Re}_{\theta_c}}.\tag{4}$$

The streamwise triggering function,  $F_{\text{onset,s}}$ , is determined by an algebraic expression for  $\text{Re}_{\theta_c}$  that depends on the turbulence intensity level,  $Tu_L$  and the pressure gradient,  $\lambda_{\theta_L}$ , calculated using local variables as follows:

$$Tu_L = \min \left[ 100 \frac{\sqrt{2k/3}}{\omega d_w}, 100 \right], \quad \lambda_{\theta_L} = -0.1111 \frac{dV}{dy} \frac{d_w^2}{\nu} + 0.1875.$$
 (5)

## 2.2. Liu et al., 2021

Liu et al. [5] in 2021 used the LCTM framework to propose a fully local three-equation transition model for hypersonic flows. Their model takes into account different transition mechanisms, including streamwise instability, nose-bluntness effects, and crossflow-induced transition. Similar to the MODEL-2B, the function  $F_{\text{onset}}$  is evaluated in this case by determining the maximum value between the streamwise and crossflow contributions, calculated as follows:

$$F_{\text{onset,s}} = \frac{\text{Re}_V}{f(\text{Ma}_{eL}, T_{eL})\text{Re}_{\theta_c}}.$$
 (6)

In the streamwise triggering function,  $F_{\rm onset,s}$ , the component  $f({\rm Ma}_{eL},T_{eL})$  is based on self-similar compressible boundary layer profiles obtained without streamwise pressure gradient. These profiles are parameterized through local estimations of Mach and temperature at the boundary layer's edge. Conversely, the value of  ${\rm Re}_{\theta_c}$  is obtained through an algebraic correlation that depends on the local turbulence intensity level  $Tu_L$ .

#### 3. Models validation

The validation of transition models is a fundamental step to assess their predictive capability across a range of canonical and applied hypersonic flow configurations. While simplified geometries, such as the flat plate, provide reference cases for isolating the effects of Reynolds number and turbulence intensity, more complex models are required to evaluate the robustness of transition correlations under realistic aerodynamic conditions. In this section, three complementary benchmarks are considered: the hypersonic flat plate, the BOLT configuration, and the Hypersonic Inflatable Aerodynamic Decelerator (HIAD) aeroshell. Together, these cases cover increasing levels of flow complexity, from two-dimensional boundary-layer development to three-dimensional effects induced by surface curvature and leading-edge sweep, thus providing a comprehensive framework to evaluate the applicability of the intermittency-based transition models.

## 3.1. Flat plate at different Reynolds numbers

The first validation case concerns the canonical hypersonic flat plate, which represents a standard configuration to assess the ability of transition models to capture the effect of varying Reynolds numbers on the boundary layer evolution. Following the procedure outlined by Liu et al. [5], simulations were performed for a flat plate of 1500 mm in length, with free-flow conditions corresponding to Mach numbers in the hypersonic regime and Reynolds numbers in the range of  $10^6-10^7$  m<sup>-1</sup>, consistent with the

**Table 1.** Flow conditions for selected flat plate cases.

Test	$Ma_\infty$	$P_\infty$ [Pa]	$T_\infty\left[K ight]$	$Re_{\infty}[1/m]$
Α	6.10	2800	570.00	$4.90 \times 10^{6}$
В	6.20	5400	690.00	$2.60 \times 10^{6}$
С	6.30	12,100	800.00	$1.70 \times 10^{6}$

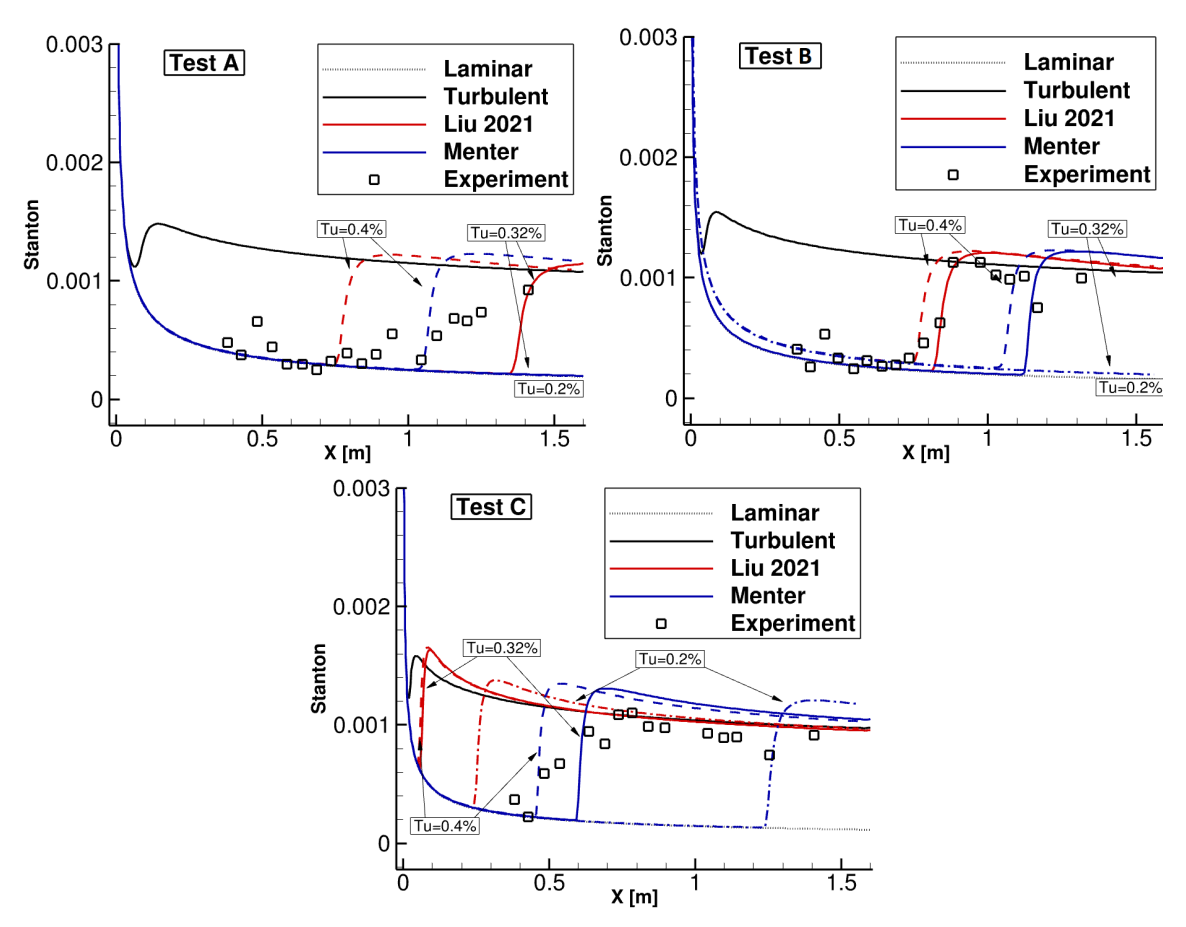


**Fig 1.** Predicted Stanton number distributions for flat plate test cases corresponding to tests A, B, and C in Table 1. The laminar curve is not always visible due to overlap with other lines.

experimental research of Mee [7]: a brief summary of these flow conditions is reported in Table 1. The wall was kept isothermal at temperature  $T_w=300$  K, consistent with the reference study. Cases were run with turbulence intensity levels of 0.20%, 0.32%, and 0.40% in order to assess the impact of turbulence intensity (Tu) on the transition. The ratio  $\mu_t/\mu$  was kept constant at 10 in all simulations. The computational grid was refined in the wall-normal direction to ensure  $y^+<1$ , while the streamwise resolution was chosen to properly capture the transition front.

The main quantity of interest is the Stanton number St, which provides direct information about the onset and development of transition (Figure 1). In line with [5], the intermittency-based model reproduces the laminar regime with good accuracy, while clear differences emerge in the transitional zone. The Smirnov–Menter model systematically predicts the turbulent region with an higher St number compared to experimental data and a delayed transition for cases A and B; for Test A, the transition is even absent (except for Tu = 0.4%). The Liu et al. model predicts a slightly delayed transition for Test A at low Reynolds number, accurately captures the transition in Test B, and predicts an early transition at the leading edge in Test C, resulting in an effectively always turbulent flow. This behavior is inconsistent

with experimental observations, which indicate that transition should occur approximately 0.4 m from the leading edge.

In all examined cases, the transition occurs almost immediately, with a sharp change from laminar to turbulent flow. Under the present assumptions, the transitional regime is therefore not predicted accurately by this method.

As anticipated, for Test C the Liu et al. model predicts a fully turbulent flow under the present assumptions. An assumption that may be particularly strong is the choice of  $\mu_t/\mu=10$ . For this test, additional simulations were therefore carried out by varying the value of  $\mu_t/\mu$  (Figure 2). As expected, decreasing this ratio shifts the transition downstream. Thus, it is possible to identify the value of  $\mu_t/\mu$  that yields a transition location consistent with the experimental data; in this case, the corresponding value is  $\mu_t/\mu=0.8$ .

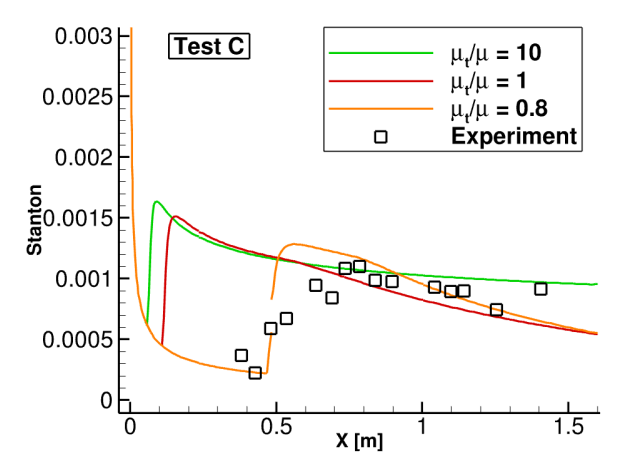


**Fig 2.** Comparison of predicted Stanton number distributions for Test C using the Liu et al. model with different values of  $\mu_t/\mu$ .

To further validate these observations, it would be beneficial to have access to additional experimental test cases and to perform further simulations. In particular, it remains to be assessed whether the appropriate inlet value of  $\mu_t/\mu$  depends systematically on the free-stream Reynolds number.

#### 3.2. **BOLT**

Shown in Figure 3, the BOLT (BOundary Layer Transition) was conceived to study hypersonic boundary-layer transition over a low-curvature concave surface with highly swept leading edges. Its geometry—featuring concave surfaces and swept edges—was deliberately designed to generate complex flow fields where multiple instability mechanisms, including second-mode and crossflow, can interact. Compared with simplified geometries, this makes the configuration a more representative platform for investigating boundary-layer transition and for validating predictive tools.

A full-scale BOLT model underwent extensive testing in the LENS-II hypervelocity reflected shock tunnel at CUBRC, and the present simulations adopt as reference the conditions of RUN-03 reported in [1]. The key parameters are: free-stream Mach number M=5.17, model-length Reynolds number  ${\rm Re}_L=3.92\times10^6$  (based on the model's length of 0.86 m), stagnation pressure of 1.5 MPa, and stagnation temperature of 1130 K, with the wall held at 294.4 K. In LENS-II, the free-stream noise has typically been measured within a 3–5% range [12]; following the methodology in [15], this corresponds to an estimated turbulence intensity between 0.42% and 0.7%. To further examine the role of free-stream turbulence on transition onset, the simulations broaden this range by considering four turbulence intensity levels, Tu=0.1,0.3,0.5, and 1.0%.

Taking advantage of the inherent forebody symmetries, only one quarter of the geometry was represented in the computational mesh. Two shock-fitted, structured multi-block meshes were generated

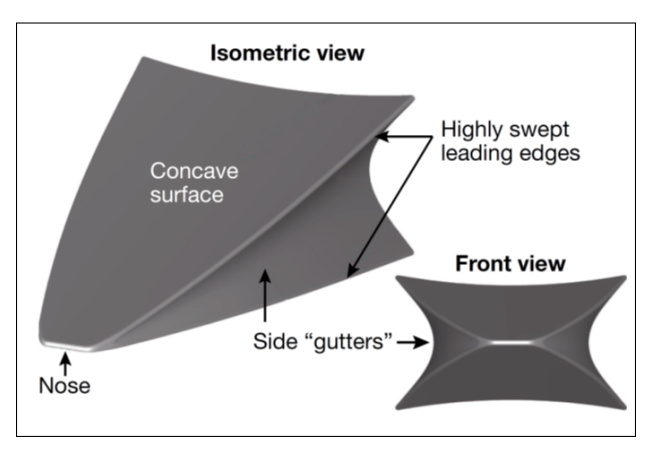


Fig 3. BOLT geometry, from [1].

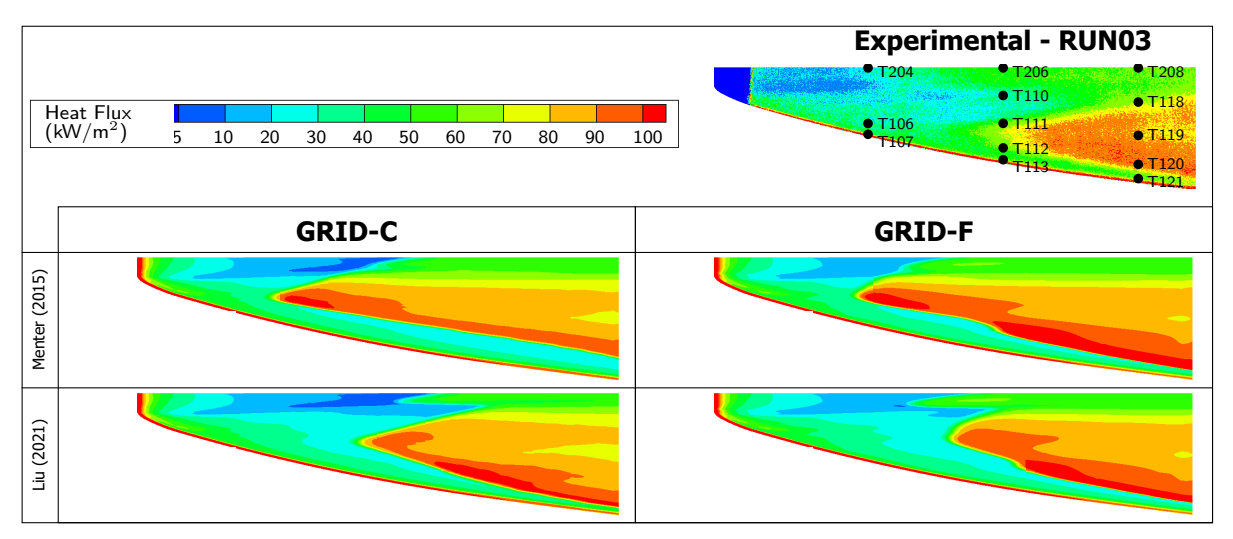
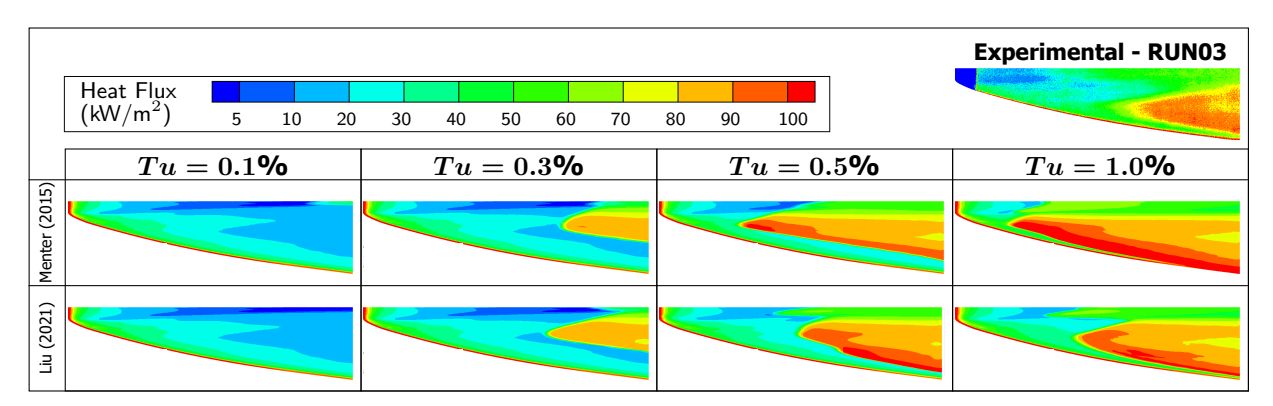


Fig 4. Mesh sensitivity analysis, Tu=0.5% and  $\mu_t/\mu=10$ .

with Ansys® IcemCFD®, consisting of 3.5 million and 24 million cells, hereafter referred to as GRID-C (coarse) and GRID-F (fine), respectively. Both meshes were clustered at the wall to ensure  $y^+ < 1$ . Figure 4 presents a comparison between solutions obtained on both grid levels for the Menter 2015 model (top rows) and the Liu 2021 model (bottom rows), in reference to experimental data from Thermal Sensitive Paint (top-right corner)[1]. Given the limited differences observed between the coarse and fine meshes, all subsequent analyses were performed using GRID-C.

Figure 5 shows the sensitivity of the predicted surface heat flux distributions to variations in the freestream turbulence intensity (Tu), compared against the experimental reference obtained from TSP. The contours represent wall heat flux levels, where the onset of laminar-to-turbulent transition is clearly identified by a sharp increase in heat flux. Overall, the simulations exhibit a pronounced dependence on the turbulence intensity, while retaining qualitative agreement with the experimental data. At Tu = 0.1%, transition is not observed, whereas at Tu = 0.3% it appears significantly delayed compared to the measurements. Improved agreement is achieved at Tu = 0.5%, while at Tu = 1.0% the transition occurs prematurely. A comparison between the turbulence models highlights that the Menter (2015) formulation is more sensitive to variations in Tu than the Liu (2021) model. Specifically, for the Menter (2015) model, the predicted transition location shifts markedly between Tu = 0.5% and Tu = 1.0%, whereas the Liu (2021) model shows only minor changes across the same range. Nevertheless, in all cases the Menter (2015) model tends to predict an earlier transition onset relative to Liu (2021).



**Fig 5.** Sensitivity to free-stream turbulent intensity level with  $\mu_t/\mu=10$ , GRID-C mesh level.

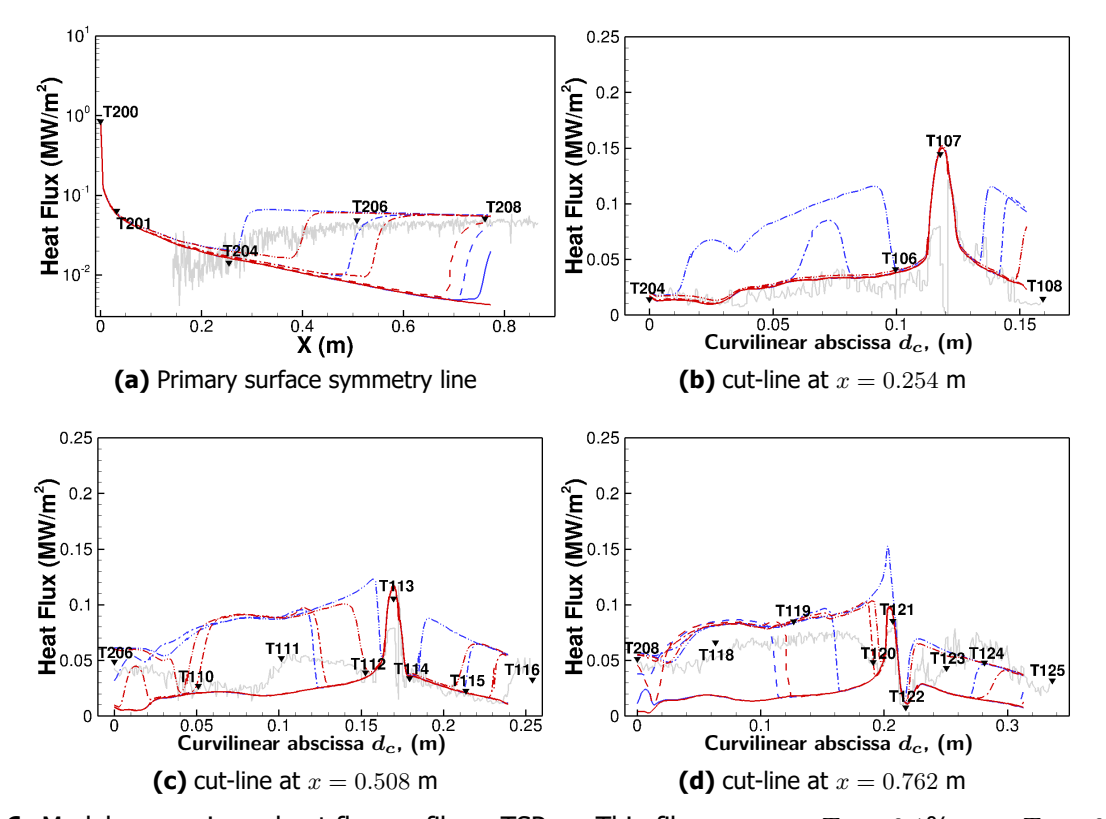


**Fig 6.** Model comparison: heat flux profiles . TSP —, Thin films  $\P, -\cdots - Tu = 0.1\%$ ,  $-\cdot - Tu = 0.3\%$ , - - Tu = 0.5%, — Tu = 1%. Colors: blue = Menter (2015), red = Liu (2021).

The aforementioned tendency becomes more apparent in Fig.6, which presents a quantitative comparison between the experimental and numerical heat flux profiles along the main symmetry line and three transverse cut lines. Results are shown for Menter (2015) in blue and Liu (2021) in red, across the four freestream turbulence levels considered. When examining the TSP-extracted profiles (light grey) on the same graphs, it is evident that the experiment displays a gradual increase in heat flux, corresponding to an extended transition zone of approximately  $0.3\,\mathrm{m}$ . In contrast, the simulations predict a much sharper transition, with the onset shifting upstream as the freestream turbulence intensity decreases. Notably, for the BOLT configuration, the Menter (2015) model predicts transition slightly earlier than Liu (2021), a trend opposite to that observed in the flat plate cases.

<b>Table 2.</b> Flow conditions for	or HIAD scal	lop-10 test cases	s at AoA = $0^{\circ}$ .
-------------------------------------	--------------	-------------------	--------------------------

Test	Mach	Re [1/m]	$T_\infty$ [K]	$ ho_\infty$ [Kg/m $^3$ ]	Tu $_{\infty}$ [%]
Α	5.96	$6.89 \times 10^{6}$	61.9	0.0325	0.1683
В	5.99	$9.94 \times 10^{6}$	62.5	0.0471	0.1534
С	6.01	$12.7 \times 10^{6}$	63.3	0.0605	0.1434

# 3.3. Hypersonic Inflatable Aerodynamic Decelerator aeroshell (HIAD) at different Reynolds numbers

The Hypersonic Inflatable Aerodynamic Decelerator (HIAD) is a deployable aeroshell concept designed to increase drag area during atmospheric entry while maintaining a lightweight structure [2]. The HIAD geometry consists of a toroidal stacked-torus structure that can be tailored through the number of tori and scalloping patterns. In experimental campaigns conducted at NASA Langley, several tests were performed by varying the scallop geometry, Reynolds number, and angle of attack. These tests provide a rich dataset for validating transition models on complex curved surfaces with significant three-dimensional effects.

The present validation focuses on the three cases reported by Liu et al. [6], corresponding to the scallop-10 configuration at zero angle of attack. This dataset is particularly valuable as it allows for testing transition models under different free-stream Reynolds numbers while maintaining a consistent geometry. The main comparison quantity is the ratio  $h/h_{fr}$ , defined as the normalized surface heat flux with respect to the fully rough turbulent reference value  $h_{fr}$ , as reported in the NASA test documentation [2]. In each case, simulations were carried out with NExT under laminar, fully turbulent, and transitional assumptions. For the transitional computations, both the Menter (2015) and Liu (2021) intermittency-based models were employed. Results are compared with the experimental measurements and with the Liu (2020) simulations available in the literature. To reduce carbuncle instabilities, the AUSM[4] scheme was adopted instead of FDS[11]. The turbulence viscosity ratio at the inflow was set to  $\mu_t/\mu=10$ . For this test case a grid of about 700.000 elements has been generated with GridPro, keeping the  $y^+<1$  at the wall.

The results for Test A (Figure 7), corresponding to the lowest Reynolds number, indicate that the Liu (2021) model predicts transition slightly earlier than the experiment (at 30 mm from the nose versus 35 mm). The transition appears abrupt, with the Stanton number rising directly from laminar to turbulent levels, a trend also observed experimentally at a different location. The Menter model predicts the laminar regime well, but around the transition it no longer follows either the laminar or the turbulent curve consistently, leading to unreliable Stanton number values. Compared with Liu (2020), the present simulations show some discrepancies in capturing the low peaks in the valleys of the scalloped geometry, though these are not well resolved even by the fully turbulent solution. This suggests that the differences may be related to the AUSM scheme or the asymptotic value of  $\mu_t/\mu$  rather than the transition model itself. Overall, the Liu (2020) results appear closer to the experimental data.

For Test B (Figure 9), the Liu (2021) model predicts transition at the correct location and exhibits behavior similar to Test A, with an abrupt change across transition. In this case, the Menter model fails to predict transition, maintaining a fully laminar solution throughout. The Liu (2020) model again shows slightly better agreement with the experimental results.

Test C (Figure 11) corresponds to the highest Reynolds number. Here, the Liu (2021) model performs very well, accurately capturing both the transition onset and the transitional region. The post-transition Stanton number distribution matches closely with the experimental measurements. The comparison with the Liu (2020) results also shows good consistency, confirming the robustness of the more recent correlation at higher Reynolds conditions.

These HIAD cases demonstrate the potential of the Liu (2021) model to capture transition behavior over complex three-dimensional geometries, though further studies are warranted to examine sensitivity to turbulence intensity levels, numerical schemes, and inflow conditions.

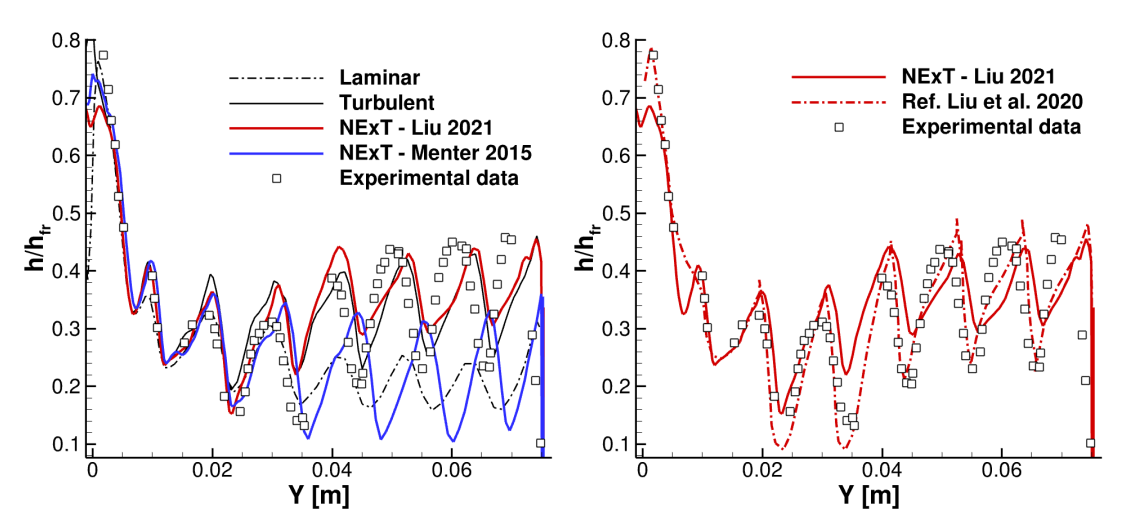


**Fig 7.** Predicted  $h/h_{fr}$  distributions on HIAD symmetry plane corresponding to case A in Table 2.

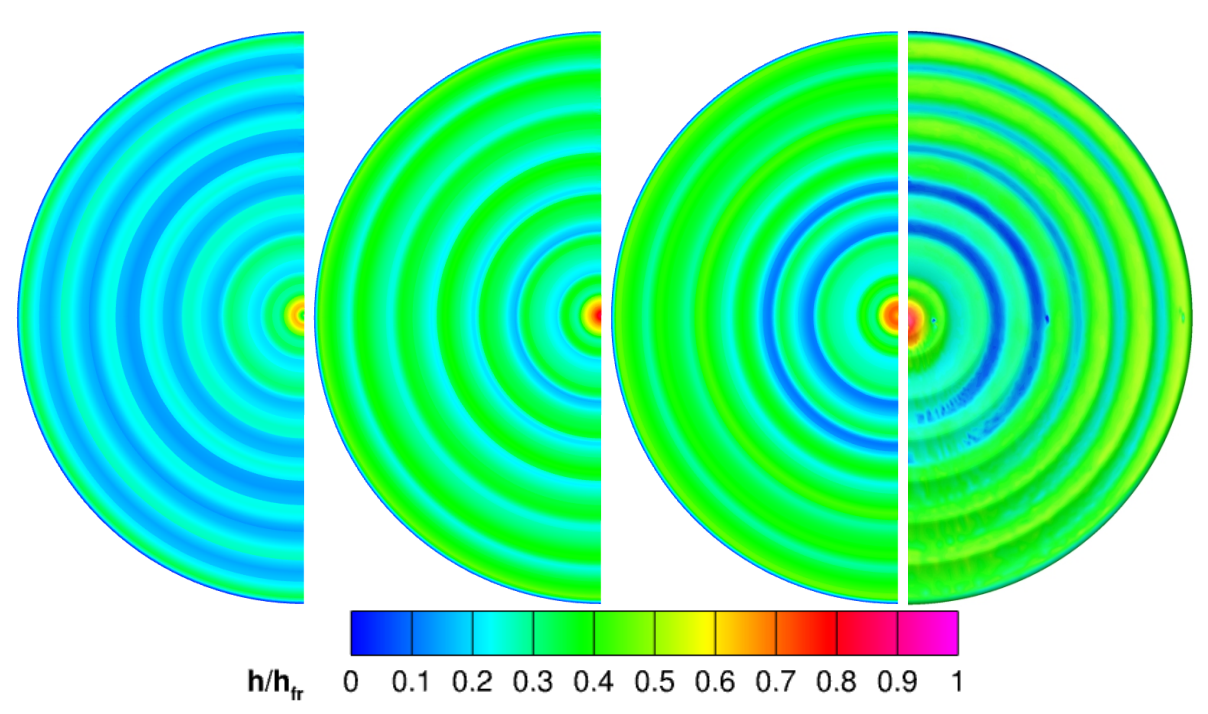


**Fig 8.** Distribution of  $h/h_{fr}$  on HIAD surface corresponding to case A in Table 2. From left to right: laminar, turbulent, transitional (Liu-2021) and Experimental contours.

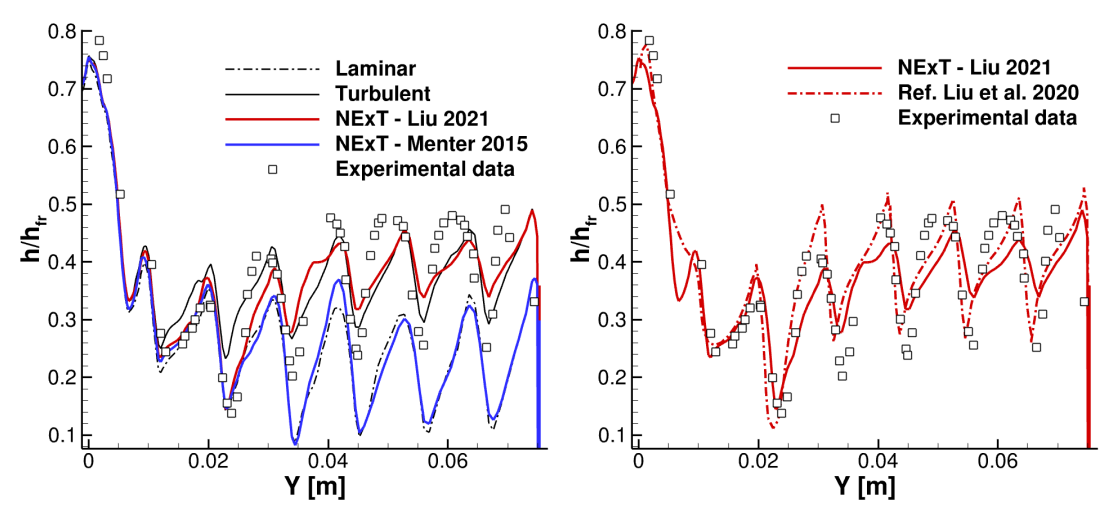


**Fig 9.** Predicted  $h/h_{fr}$  distributions on HIAD symmetry plane corresponding to case B in Table 2.

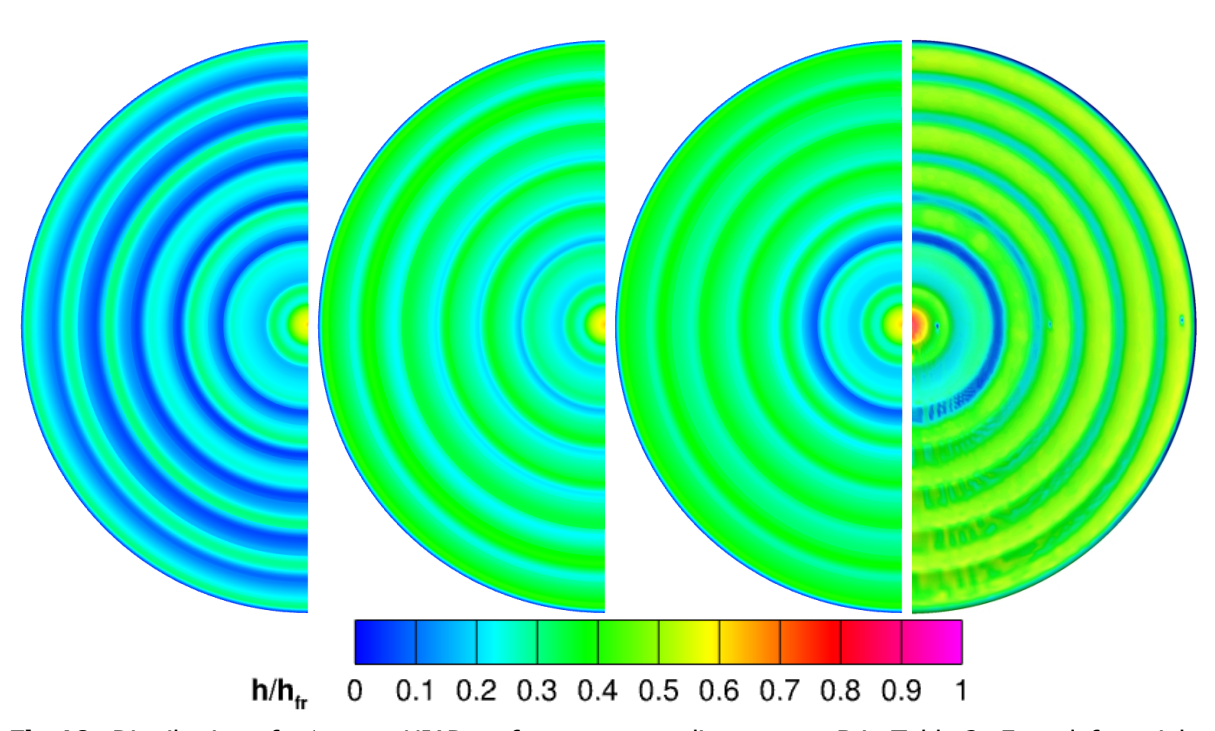


**Fig 10.** Distribution of  $h/h_{fr}$  on HIAD surface corresponding to case B in Table 2. From left to right: laminar, turbulent, transitional (Liu-2021) and Experimental contours.

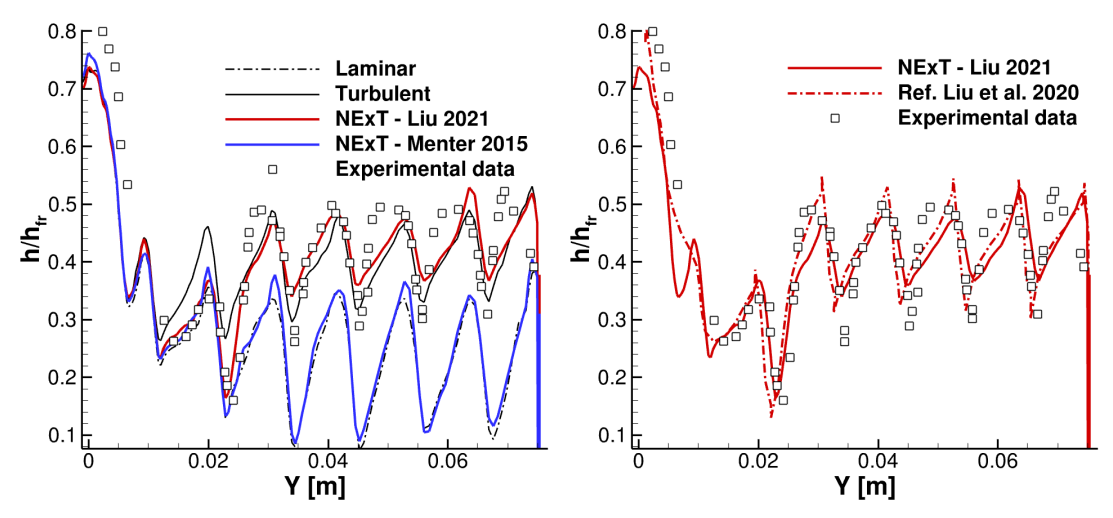


**Fig 11.** Predicted  $h/h_{fr}$  distributions on HIAD symmetry plane corresponding to case C in Table 2.

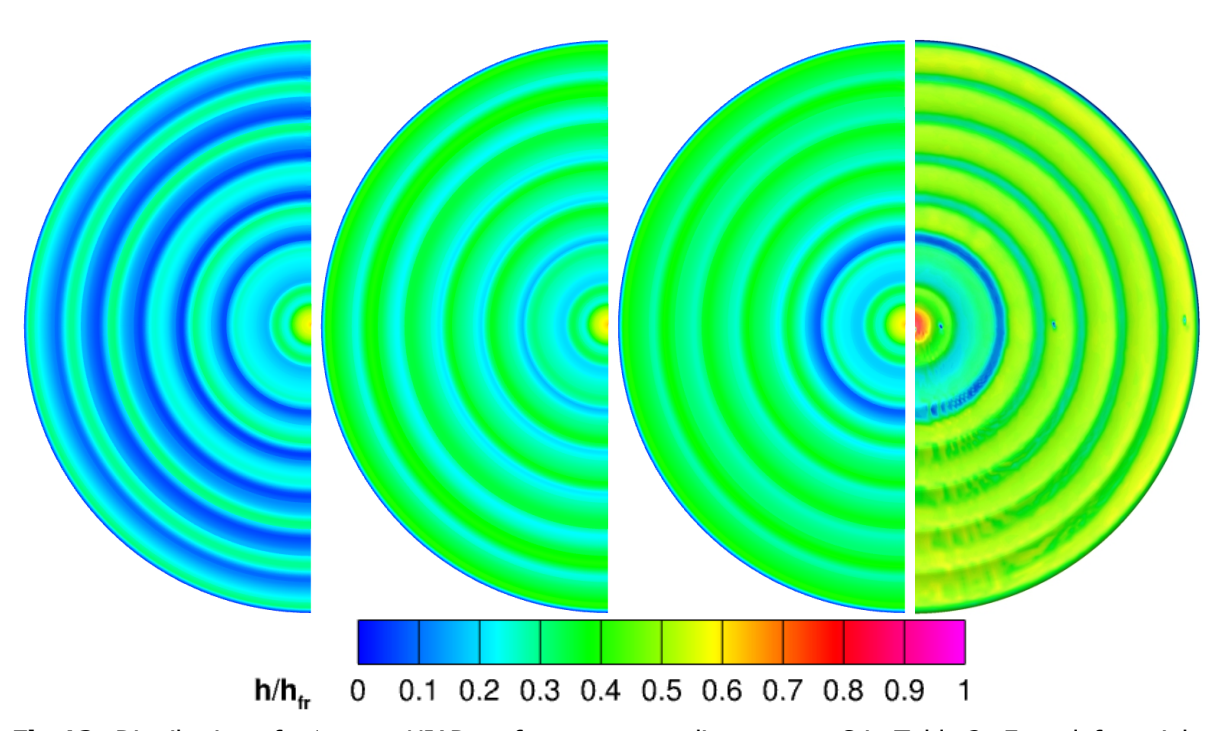


**Fig 12.** Distribution of  $h/h_{fr}$  on HIAD surface corresponding to case C in Table 2. From left to right: laminar, turbulent, transitional (Liu-2021) and Experimental contours.

#### 4. Conclusions

The present study has investigated the performance of intermittency-based transition models within a RANS framework for predicting boundary-layer transition in hypersonic flows. Two representative formulations, namely the Smirnov–Menter (2015) model and the Liu et al. (2021) model, have been assessed across canonical and applied configurations, including the hypersonic flat plate, the BOLT demonstrator, and the HIAD aeroshell.

For the flat plate cases, both models were able to capture transition in most conditions, with the Smirnov–Menter model generally predicting a delayed location. Both formulations, however, produced a transition that was too sharp, whereas experimental data indicate a smoother progression from laminar to turbulent flow. Sensitivity studies highlighted the strong influence of the turbulence viscosity ratio at the inflow, suggesting that calibration of this parameter is crucial for quantitative agreement with experiments.

The BOLT configuration offered a more challenging assessment of model robustness under complex three-dimensional flow effects. Both transition models remained sensitive to free-stream turbulence intensity, although the Liu et al. model tended to become less responsive at higher Tu levels. For this test case, the Smirnov–Menter model generally predicted transition slightly upstream relative to the Liu et al. model.

The HIAD aeroshell test cases further emphasized these differences. At low Reynolds numbers, the Liu (2021) model slightly anticipated transition, while the Smirnov–Menter model failed to reproduce transition in some cases. At higher Reynolds numbers, the Liu (2021) model demonstrated improved predictive capability, accurately capturing both transition onset and post-transition behavior, in good agreement with experimental data.

Overall, the results confirm the potential of intermittency-based transition models for engineering applications in hypersonic regimes, while also highlighting important limitations. The strong dependence on inflow parameters such as turbulence intensity and viscosity ratio underscores the need for careful calibration and sensitivity analyses. Moreover, the inability of the models to reproduce extended transition regions points to inherent limitations of the current formulations. Future work should therefore focus on refining local correlations, improving the treatment of free-stream disturbances, and incorporating additional physical mechanisms such as non-equilibrium effects and surface roughness. These advancements are expected to enhance the robustness of RANS-based transition modeling for realistic hypersonic vehicle design.

#### References

- [1] Dennis C. Berridge, Gregory McKiernan, Tim P. Wadhams, Michael Holden, Bradley M. Wheaton, Thomas D. Wolf, and Steven P. Schneider. Hypersonic ground tests in support of the boundary layer transition BOLT flight experiment. In AIAA Paper 2018-2893, 2018.
- [2] Brian R. Hollis. Experimental aerothermal heating for hypersonic inflatable aerodynamic decelerator configurations. NASA Technical Memorandum NASA/TM–2017-219585, NASA, Langley Research Center, Hampton, Virginia, June 2017.
- [3] Robin B. Langtry and Florian R. Menter. Correlation-based transition modeling for unstructured parallelized computational fluid dynamics codes. AIAA Journal, 47(12):2894–2906, 2009.
- [4] M. S. Liou. A further development of the AUSM+ scheme towards robust and accurate solutions for all speeds. In AIAA Paper 2003-4116, Orlando, FL, June 2003.
- [5] Z. Liu, Y. Lu, J. Li, and C. Yan. Local correlation-based transition model for high-speed flows. AIAA Journal, 60(3):1365–1381, 2022.
- [6] Zaijie Liu, Steven J. Beresh, Joseph W. Nichols, Meelan Choudhari, and Ramesh K. Agarwal. A fully local correlation-based transition model for hypersonic flows. Aerospace Science and Technology, 105:106055, 2020.

- [7] David J. Mee. Boundary-layer transition measurements in hypervelocity flows in a shock tunnel. AIAA Journal, 40(8):1542–1548, 2002.
- [8] F. R. Menter. Two-equation eddy-viscosity turbulence models for engineering applications. AIAA Journal, 32(8):1598–1605, 1994.
- [9] F. R. Menter and P. Smirnov. Development of a RANS-based model for predicting crossflow transition. In Proceedings of the contributions to the 19th STAB/DGLR symposium, 2014.
- [10] Florian R. Menter, Pavel E. Smirnov, Tao Liu, and Ravikanth Avancha. A one-equation local correlation-based transition model. Flow, Turbulence and Combustion, 95(4):583–619, Dec 2015.
- [11] M. Pandolfi and S. Borrelli. An Upwind Formulation for Hypersonic Non-equilibrium Flows. Modern Research Topics in Aerospace Propulsion. Springer-Verlag, 1991.
- [12] Philippe Portoni. Personal communication, 2023.
- [13] J. Steelant and E. Dick. Modeling of bypass transition with conditioned Navier–Stokes equations coupled to an intermittency transport equation. International Journal for Numerical Methods in Fluids, 23:193–220, 1996.
- [14] Y. B. Suzen and P. G. Huang. Modeling of flow transition using an intermittency transport equation. Journal of Fluids Engineering – Transaction of ASME, 122:273–284, 2000.
- [15] Liang Wang, Lianghua Xiao, and Song Fu. A modular RANS approach for modeling hypersonic flow transition on a scramjet-forebody configuration. Aerospace Science and Technology, 56:112–124, 2016.